Graphite in the bi-layer regime: in-plane transport

D. B. Gutman,[1,2] S. Tongay,[3] H. K. Pal,[3] D. L. Maslov,[3] and A. F. Hebard[3]

[1] *Institut für Theorie der kondensierten Materie, Universität Karlsruhe, 76128 Karlsruhe, Germany*
[2] *DFG–Center for Functional Nanostructures, Universität Karlsruhe, 76128 Karlsruhe, Germany*
[3] *Department of Physics, University of Florida, Gainesville, FL 32611, USA*
(Dated: July 2, 2009)

An interplay between the increase in the number of carriers and the decrease in the scattering time is expected to result in a saturation of the in-plane resistivity, ρ_{ab}, in graphite above room temperature. Contrary to this expectation, we observe a pronounced increase in ρ_{ab} in the interval between 300 and 900 K. We provide a theory of this effect based on intervalley scattering of charge carriers by high-frequency, graphene-like optical phonons.

PACS numbers: 81.05.Uw, 72.10-d

I. INTRODUCTION

The family of graphite allotropes includes fullerenes, carbon nanotubes, graphene, graphite, and diamond. A combination of chemical simplicity and diverse physical properties, characteristic for these materials, makes carbon-based electronics a promising field of research. Surprisingly, many properties of the most common member of this group, graphite–such as non-metallic c-axis transport[1] and apparent quantization of Hall resistance[2]– are yet to be explained. In this work, we focus on in-plane transport in graphite at zero magnetic field, which is well understood in the degenerate regime, i.e., for $T < E_F \sim 250$ K (we set $k_B = \hbar = 1$).[1] Extending the upper limit of the temperature range to 900 K, we observe an unexpected pronounced increase in the in-plane resistivity. We explain this effect by interaction of carriers with high-frequency, graphene-like optical phonons.

The band structure of graphite can be characterized by three energy scales.[1] The largest one is set by the hopping matrix element between A and B atoms in graphene sheets: $\gamma_0 \approx 3.2$ eV. The next two largest ones comprise the matrix elements between adjacent Bernal-stacked graphene sheets: $\gamma_1 \approx 0.35$ eV (for the vertical bond) and $\gamma_3 \approx 0.3$ eV (for the slanted bond). Next comes a large number of matrix elements between next-to-nearest neighbors, which are known to less accuracy, but are generally believed not to exceed several tens of meV. The major difference between graphite and graphene, i.e., an overlap of the conduction and valence band which gives rise to a small ($\approx 3 \times 10^{18}$ cm^{-3} at $T \to 0$) but finite carrier concentration, is due to hopping between next-to-nearest planes. The band overlap and the Fermi energy are on the order of this matrix element. Prior transport measurements of graphite were performed at or below 300 K, where it behaves as a compensated semi-metal with finite Fermi energy. There is, however, a very interesting but hitherto unexplored regime of temperatures $E_F \lesssim T \lesssim \gamma_1 \approx 4060$ K. This regime can be viewed as a critical region of the quantum phase transition between a semi-metal with finite band overlap and a semiconductor with finite band gap. Since next-to-nearest plane couplings are irrelevant in this regime, graphite can be

thought of as a stack of graphene bi-layers.[4] We dub this regime as "bi-layer graphite" (BLGT). If slanted hopping (γ_3) is also neglected, BLGT is described by a simple (and historically the first) Wallace model of graphite,[3] which contains only two hoppings: γ_0 and γ_1. The energy spectrum in this model consists of two electron and two hole branches

$$\varepsilon_{\mathbf{k}} = \pm\gamma_1\Gamma \pm \sqrt{\gamma_1^2\Gamma^2 + \gamma_0^2|S_{\mathbf{k}}|^2}, \qquad (1)$$

where $\Gamma = \cos{(k_z c/2)}$, c is the c-axis lattice constant and $S_{\mathbf{k}}$ is the structure factor for hopping between inequivalent (A and B) atoms:

$$S_{\mathbf{k}} = e^{ik_x a/\sqrt{3}} + 2e^{-ik_x a/2\sqrt{3}}\cos(ak_y/2). \qquad (2)$$

Near the K and K' points of the Brillouin zone, $\gamma_0 S_{\mathbf{k}} \approx v_0\xi_{\mathbf{k}} \equiv v_0(k_x + ik_y)$, where v_0 is the Dirac velocity of a single graphene layer. The density of states in BLGT is energy-independent $\nu = 16\gamma_1/v_0^2 c$ up to $\mathcal{O}(\varepsilon/\gamma_1)$ terms (Ref. 3). Consequently, the number density of charge carriers increases linearly with T and the in-plane conductivity scales linearly with $T\tau$ (Ref. 3)

$$\sigma_{ab} = (4\ln 2/\pi)\,(e^2/c)\,T\tau. \qquad (3)$$

At high temperatures, when scattering is predominantly due to phonons, one expects $1/\tau$ to scale linearly with T and, consequently, σ_{ab} to be T independent. The conductivity measured previously up to 300K does indeed show a tendency to saturation,[1] in accord with this expectation. However, a different behavior is observed for $T > 300$K.

II. EXPERIMENT

We measured the in-plane resistivity of highly oriented pyrolytic graphite (HOPG) from 290 K up to 900 K in a sealed oven and from 1.7 K up to 310 K in Physical Property Measurement System (PPMS) using LR700 16 Hz AC resistance bridge in four terminal contact configuration. The samples were cleaved before measurements. Reproducibility of the results was checked by superimposing the temperature-dependent resistivities of

two separate samples (Fig. 1 inset). All HOPG samples were identified to have 0.5 degree mosaic spread determined by X-ray rocking curve measurements. Gold contacts to the sample were made using silver or graphite paint. Reproducibility of the measurements was checked by sweeping the temperature up and down in the range $1.7\ \mathrm{K} \le T \le 900\ \mathrm{K}$. High temperature measurements were performed in a sealed oven with nitrogen flowing gas. Temperature was recorded by a type J thermocouple located $\sim 1\mathrm{mm}$ from the sample to minimize temperature lagging effects. Each data point was taken after reaching temperature stability. The room temperature resistivity was measured to be $\rho_{ab}^{300\mathrm{K}} \approx 32\ \mu\Omega\cdot\mathrm{cm}$ before and after annealing, consistent with the existing literature values.[1] Since $\rho_{ab}^{300\mathrm{K}}$ remains at the same value before and after annealing, we conclude that adsorption/desorption of impurities or doping does not occur up to 900 K. In addition, X-ray photoelectron spectroscopy (XPS, Fig. 2a) and Auger electron spectroscopy (AES, Fig. 2b) were performed on different samples and contamination was not observed. The XPS and AES spectra displayed respectively a characteristic C1s peak at 284.6 eV and a C auger peak at 271.8 eV. The shape and position of the XPS C1s peak was unaltered indicating that C remained in the same chemical state. When relating the measured resistance to resistivity, the lattice constant was assumed to be constant. We estimate the change of the c-axis lattice constant to be 1% at the highest temperature measured.[5,6]

The experimental results for $\rho_{ab}(T)$ are presented in Fig. 1 as points. Note that the tendency to saturation pronounced at $T \sim 300$ K is superseded by a rapid increase which continues unabated up to the highest temperature measured. The dashed line in the top panel shows the theoretical prediction for $\rho_{ab}(T)$, calculated for $1/\tau = 1/\tau_0 + \alpha T$ and for a realistic energy spectrum of carriers. While this model describes the experiment at low temperatures, it fails completely for $T > 300$ K. A slow increase in the theoretical curve, which amounts only for a $\sim 12\%$ increase of ρ_{ab} from 300 to 900 K, is due to corrections of order T/γ_1 to Eq. (3).

III. THEORY

To explain the observed T-dependence of ρ_{ab}, we first notice that the highest resistivity measured, $\rho_{ab}^{895\mathrm{K}} \approx 62.5\ \mu\Omega\cdot\mathrm{cm}$, corresponds to 2 k$\Omega$ per graphene sheet, i.e., well below the resistance quantum, $h/e^2 \approx 25$ kΩ. Therefore, the Boltzmann equation should provide an adequate description of transport in the entire temperature interval. To explain the data, we thus need to invoke a new scattering mechanism, with $1/\tau$ increasing faster than T.
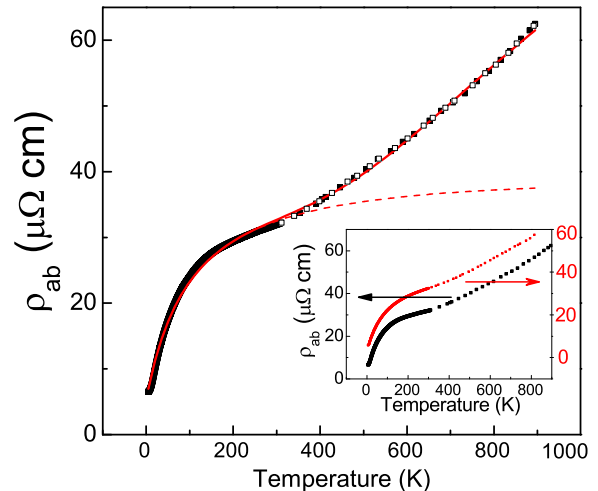

FIG. 1: (Color online). Measured temperature dependence of the in-plane resistivity of HOPG for warming (filled squares) and cooling (blank squares) temperature sweeps. Dashed: theoretical prediction for $\rho_{ab}(T)$ in the model containing scattering at impurities and soft phonons. Solid: fit using the model containing scattering at impurities, soft phonons, and intervalley scattering at hard in-plane optical phonons [Eq. (17)]. Inset: overlap of the data for two different samples. The vertical scales were shifted for clarity.

A. Qualitative picture of transport

Before proceeding with a discussion of such mechanisms, it is instructive to develop a more intuitive picture of transport in BLGT. To this end, we replace the Wallace spectrum by a massive (Galilean) form obtained by expanding Eq. (1) in $k_{||} \equiv \sqrt{k_x^2 + k_y^2}$ and keeping only the degenerate branches of electrons and holes:

$$\varepsilon_{\mathbf{k}}^{\pm} = \pm k_{||}^2/2m_{||}(k_z),\qquad (4)$$

where $m_{||}(k_z) = \Gamma\gamma_1/v_0^2$ is the k_z-dependent mass of the in-plane motion. Evaluating the in-plane conductivity as

$$\sigma_{ab}(T) = 4e^2 \int d^3k \left(-\partial f_{\mathbf{k}}^0/\partial\varepsilon_{\mathbf{k}}\right) v_{||}^2 \tau\left(\varepsilon_{\mathbf{k}}, T\right)/(2\pi)^3\ (5)$$

with spectrum given by Eq. (4), $\tau = \mathrm{const}$, and $f_{\mathbf{k}}^0 = 1/\left(\exp\left(\varepsilon_k/T\right) + 1\right)$, we reproduce Eq. (3). Typical momenta contributing to σ_{ab} are $k_z \sim 1/c$ and $k_{||} \sim k_T \equiv \sqrt{2\bar{m}_{||}T}$, where $\bar{m}_{||} \equiv m_{||}(k_z = 0) = \gamma_1/v_0^2$. Although expansion in $k_{||}$ breaks down near the H points ($k_z = \pm\pi/c$), where Γ vanishes and the spectrum is Dirac-like, the contribution of Dirac fermions to σ_{ab} is small in proportion to the volume of the Brillouin zone they occupy.[7] Therefore, a typical carrier (in zero magnetic field) in BLGT is massive rather than Dirac-like and the isoenergetic surfaces are corrugated cylinders
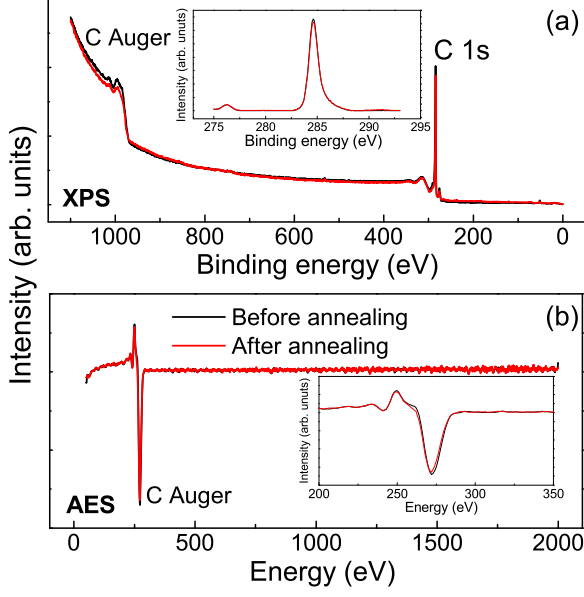
FIG. 2: (Color online). (a) X-ray photoelectron spectroscopy (XPS) spectra before and after annealing. (b) Auger electron spectroscopy (AES) spectra before and after annealing. Insets: magnified carbon peaks.

centered near the K points. As in the case of bi-layer graphene,[8] γ_3 hopping (responsible for trigonal warping of the isoenergetic surfaces) leads to a linear-in-$k_{||}$ term in the energy spectrum, which is smaller than the quadratic term for energies $> \gamma_1 \gamma_3^2 / \gamma_0^2 \sim 30$ K. Since we are not interested here in special effects arising solely from trigonal warping, e.g., longitudinal magnetoresistance, this term can be safely neglected.

Having this simple picture in mind, we now turn to a discussion of various scattering mechanisms.

B. Scattering mechanisms

1. Electron-hole interaction

We start with the *electron-hole* interaction. In contrast to the electron-electron interaction, this mechanism gives rise to finite resistivity in a compensated semi-metal even in the absence of Umklapp processes.[9,10] For $T \ll E_F$, we have a usual Fermi-liquid behavior $1/\tau_{\text{e-h}} \propto T^2$. The T^2-behavior of ρ_{ab} is indeed observed in graphite below 5 K.[11,12] However, BLGT is not a Fermi liquid but rather a non-degenerate electron-hole plasma with fixed (and equal to zero) chemical potential. To estimate the strength of Coulomb interaction, we calculate the r_s parameter, i.e. the ratio of typical potential and kinetic

energies

$$r_s(T) = e^2/\epsilon_\infty l E_{\text{kin}}, \qquad (6)$$

where ϵ_∞ is the background dielectric constant of graphite and $l = (4\pi/3)^{1/3} n^{-1/3} \propto T^{-1/3}$ is the typical inter-carrier distance. Using an experimentally measured values of number density $n \approx 10^{19}$ cm^{-3} at $T = 300$ K (Ref. 13) and $\epsilon_\infty \approx 5$ (Ref. 14) and evaluating the kinetic energy as $E_{\text{kin}} = \left(\pi^2/12\ln 2\right) T \approx 1.2T$ (Ref. 15), we obtain $r_s(T = 300$ K$) \approx 1.2$. As temperature increases, $r_s(T)$ decreases as $T^{-2/3}$. Therefore, the perturbation theory for the electron-hole interaction is reasonably accurate already at $T \simeq 300$ K and becomes even better at higher T. In the Thomas-Fermi model, the screened Coulomb potential $U(\mathbf{q}) = 4\pi e^2/\epsilon_\infty \left(q_{||}^2 + q_z^2 + \kappa^2\right)$ is isotropic even if the electron spectrum is not; all details of the spectrum are encapsulated in the (square of) screening wavenumber $\kappa^2 = 4\pi e^2 \nu/\epsilon_\infty$ proportional to the density of states. In BLGT, κ^2 is T-independent and, since ν is proportional to the (small) in-plane mass, $\kappa \ll c^{-1}$. Also, at not too high temperatures, $k_T \propto \sqrt{T} \ll \kappa$. Since $q_{||}$ cannot exceed the typical electron momentum, $q_{||} \lesssim k_T \ll \kappa$ and $U(q)$ almost does not depend on $q_{||}$: $U(\mathbf{q}) \approx 4\pi e^2/\epsilon_\infty \left(q_z^2 + \kappa^2\right)$. Using this form of $U(q)$ and the spectrum from Eq. (4), we obtain from the Fermi Golden Rule

$$\frac{1}{\tau_{\text{e-h}}} \sim \frac{e^2 \gamma_1}{\epsilon \kappa v_0^2} T. \qquad (7)$$

This linear scaling persists even at higher temperatures ($T \gtrsim \gamma_1$), in the single-layer limit.[16] Therefore, electron-hole interaction does not provide an explanation of the experiment.

2. Electron-phonon interaction

We now turn to the *electron-phonon* scattering. With 4 atoms per unit cell, graphite has 3 acoustic and 9 optical phonon modes. The phonon spectrum consists of two groups of modes: "hard" and "soft".[17] The characteristic energy scale of hard modes, which are present already in graphene, is ~ 0.1 eV. Soft modes, with typical energies of order 10 meV, arise from weak coupling between graphene sheets. For the temperatures of interest ($T > 300$ K), all soft modes are in the classical regime, in which the occupation number and, thus, the scattering rate scale linearly with T. Although hard acoustic modes are still below their Debye temperatures, they are also in the classical regime. For example, typical in-plane phonon momenta involved in scattering at a hard, graphene-like acoustic mode with dispersion $\omega_A = s_{ab} q_{||}$ are $\bar{q}_{||} \sim \bar{k}_{||}$. The corresponding frequencies $\bar{\omega}_A \sim s_{ab} \bar{k}_{||}$ are smaller than T as long as $T \gg \bar{m}_{||} s_{ab}^2 \sim 1$ K. Therefore, all soft modes as well as hard acoustic modes lead to linear scaling of the scattering rate $\tau_{\text{e-ph}}^{-1} = \alpha T$.

The remaining hard modes are graphene-like optical phonons, e.g., the longitudinal optical (E_{2g}) mode with frequency $\omega_0 \approx 0.17$ eV at the Γ point.[17,18] For $T \lesssim \omega_0$, scattering at these modes leads to an exponential growth of the resistivity with temperature. In the remainder of the paper, we will show that this mechanism is capable of explaining the experiment.

Even if only hard phonons are taken into account, a real picture of the electron-phonon interaction in graphite is rather complicated, as both inter- and intra-valley scattering on a number of modes are involved. Since our goal is just to obtain the temperature dependence of the resistivity, we will construct a simplified model,[21,22] taking into account only inter-valley scattering due to one optical mode. We start from a tight-binding Hamiltonian

$$H_{\text{graphite}} = \begin{pmatrix} H_\parallel & H_\perp \\ H_\perp^\dagger & H_\parallel^* \end{pmatrix}. \tag{8}$$

Here, $H_\parallel$ describes hopping within graphene sheets

$$H_\parallel = \begin{pmatrix} \gamma_0' \tilde{S}_{\mathbf{k}} & \gamma_0 S_{\mathbf{k}} \\ \gamma_0 S_{\mathbf{k}}^* & \gamma_0' \tilde{S}_{\mathbf{k}} \end{pmatrix}, \tag{9}$$

where $\tilde{S}_{\mathbf{k}} = 4\cos\left(\sqrt{3}k_x a/2\right)\cos\left(k_y a/2\right) + 2\cos\left(k_y a\right)$ is the structure factor for in-plane hopping between next-to-nearest neighbors (AA and BB). As we will show shortly, the electron-phonon interaction is dominated by the coupling between the diagonal part of $H_\parallel$ and phonons. Near the K and K' points, $\tilde{S} \approx -3 + 3k_\parallel^2 a^2/4$. The momentum-dependent part of $\tilde{S}$ changes the spectrum only at large ($\sim 1/a$) $k_\parallel$ and, therefore, can be neglected. Hopping in the c-direction is described by

$$H_\perp = \begin{pmatrix} 2\gamma_1 \cos(k_z c/2) & 0 \\ 0 & 0 \end{pmatrix}. \tag{10}$$

The spectrum of Hamiltonian (8) is given by Eq.(1), while the eigenvectors are represented by a spinor $\lambda_{\mathbf{k}} = C\left(\pm\varepsilon_{\mathbf{k}}/\xi_{\mathbf{k}}, \pm 1, \varepsilon_{\mathbf{k}}/\xi_{\mathbf{k}}, 1\right)$ near the K point and by $\lambda_{\mathbf{k}}^*$ near the K' point. The elements of $\lambda_{\mathbf{k}}$ are the amplitudes of finding a charge carrier on one of the four atoms ($A, B, \tilde{A}, \tilde{B}$) of the graphite unit cell. It is important to notice a difference between $\lambda_{\mathbf{k}}$ and the graphene spinors $\mu_{\mathbf{k}} = (1, \pm\varepsilon_{\mathbf{k}}/\xi_{\mathbf{k}})$. Near the K points, $\varepsilon_{\mathbf{k}} = |\xi_{\mathbf{k}}|$ in graphene and, therefore, A and B atoms are occupied with equal probabilities. If the optical phonon frequency is much smaller than γ_1, both the initial and final states of a scattering process are described by the spectrum in Eq. (4). For this spectrum, the amplitudes on A and $\tilde{A}$ atoms are small as $|\varepsilon_{\mathbf{k}}|/|\xi_{\mathbf{k}}| \sim \bar{k}_\parallel/\bar{m}_\parallel v_0 \sim (T/\gamma_1)^{1/2} \ll 1$.[22] Neglecting these amplitudes, we replace the eigenvectors by $\lambda_{\mathbf{k}}^0 = (0, \pm 1, 0, 1)/\sqrt{2}$. In reality, $\omega_0/\gamma_1 \approx 0.5$ and corrections to the results following from this approximation would be important in a more detailed theory.

In the simplest model, phonons modulate hopping amplitudes by stretching the corresponding bonds. The

Hamiltonian of this interaction has the same structure as that for an ideal lattice

$$H_{\text{e-ph}} = \begin{pmatrix} \tilde{H}_\parallel & \tilde{H}_\perp \\ \tilde{H}_\perp^\dagger & \tilde{H}_\parallel^* \end{pmatrix}, \tag{11}$$

where tilde denote corrections to hopping matrix elements due to lattice distortions. If $\tilde{H}_\parallel$ does not have diagonal elements, the matrix element of $H_{\text{e-ph}}$ between the spinors $\lambda_{\mathbf{k}}^0$ vanishes. Therefore, the electron-phonon interaction appears only in the diagonal elements, describing modulation of hopping between the next-to-nearest neighbors. Expanding Hamiltonian (8) in atomic displacements, one finds

$$H_{\text{e-ph}}^{AA} = i\frac{\partial\gamma_0'}{\partial a}\sum_q \mathbf{F}\cdot\hat{\mathbf{u}}_{A,\mathbf{q}}$$

$$F_x = \sin aq_x + 2\sin\left(aq_x/2\right)\cos\left(\sqrt{3}aq_y/2\right)$$

$$F_y = 2\sqrt{3}\sin\left(a\sqrt{3}q_y/2\right)\cos\left(aq_x/2\right), \tag{12}$$

where $\hat{\mathbf{u}}_{A,\mathbf{q}}$ is the displacement operator for A atoms in momentum space. Displacements in the c-direction, being perpendicular to the plane, do not change (to linear order) the distance between adjacent A atoms, and are therefore uncoupled from fermions. Since the formfactors F_x and F_y are small for small q, processes with larger q have higher probabilities. For this reason, we will focus on inter-valley scattering between K and K' points, corresponding to $\mathbf{q} = \mathbf{q}_0 \equiv 2\pi/a\left(-1/\sqrt{3}, 1/3\right)$.

Further expansion in displacements generates higher-order vertices of the electron-phonon interaction which account for anharmonic effects. Although anharmonicity is important in a monolayer graphene,[19] it is weak in bulk graphite. For example, the temperature variation of the c-axis thermal expansion coefficient amounts only to 6% in the temperature interval from 273 to 1000 K.[20] Therefore, we neglect the anharmonic effects for now but will return to this point when discussing the experiment. Employing Eq. (12), we find the matrix element $M_{\mathbf{k}_1\to\mathbf{k}_2}^{\mathbf{q}} = \delta_{\mathbf{k}_2,\mathbf{k}_1+\mathbf{q}}\Upsilon_{\mathbf{q}}/\sqrt{2\rho\omega_{\mathbf{q}}L^3}$, where $\Upsilon_{\mathbf{q}} = (\partial\gamma_0'/\partial a)\mathbf{d}_{\mathbf{q}}\cdot\mathbf{F}$ is the deformation potential for optical phonons, $\mathbf{d}_{\mathbf{q}}$ is the polarization vector, L is a system size, and ρ is the mass density. The corresponding scattering time can be evaluated as[10]

$$\tau_{\text{e-ph}}^{-1}(\mathbf{k}_1) = \sum_{k_2}\left(W_{\mathbf{k}_1\to\mathbf{k}_2}^{+\mathbf{q}} + W_{\mathbf{k}_1\to\mathbf{k}_2}^{-\mathbf{q}}\right)\left(1 - f_{\mathbf{k}_2}^0\right)\left(1 - f_{\mathbf{k}_1}^0\right))^{-1}, \tag{13}$$

where the transition rates of emission and absorption of phonons, respectively, are

$$W_{\mathbf{k}_1\to\mathbf{k}_2}^{\pm\mathbf{q}} = 2\pi|M_{\mathbf{k}_1\to\mathbf{k}_2}^{\mathbf{q}}|^2\left(N_{\mathbf{q}} + \frac{1}{2}\pm\frac{1}{2}\right)\delta\left(\varepsilon_{\mathbf{k}_1} - \varepsilon_{\mathbf{k}_2}\mp\omega_{\mathbf{q}}\right), \tag{14}$$

and $N_{\mathbf{q}}$ is the Bose function. Neglecting the dispersion of the optical mode and using the simplified electron spectrum from Eq. (4), we find for the inter-valley scattering

rate

$$\tau_{\text{iv}}^{-1}(\varepsilon_{\mathbf{k}}, T) = \bar{\tau}^{-1} \frac{\coth\left(\omega_0/2T\right)\cosh^2\left(\varepsilon_{\mathbf{k}}/2T\right)}{\cosh^2\left(\varepsilon_{\mathbf{k}}/2T\right) + \sinh^2\left(\omega_0/2T\right)}, \quad (15)$$

where all model-dependent details of the electron-phonon interaction are incorporated into $\bar{\tau}^{-1}$. For a thermal electron ($\varepsilon_{\mathbf{k}} \sim T$) the scattering rate behaves as $\exp\left(-\omega_0/T\right)$ for $T \ll \omega_0$. For $T \gg \omega_0$, scattering at this mode crosses over into the classical regime and $\tau_{\text{iv}}^{-1} \sim T/\omega_0\bar{\tau}$.

At sufficiently high temperatures, where intervalley scattering is the dominant mechanism, the conductivity is obtained by substituting $\tau_{\text{iv}}(\varepsilon_{\mathbf{k}}, T)$ into Eq. (5)

$$\sigma_{ab}^{(\text{iv})} = \left[\left(4\ln 2 - 1\right)/3\pi\right]\left(e^2/c\right) T\bar{\tau}\exp\left(\omega_0/T\right), \quad (16)$$

C. Comparison to experiment

Based on the result for the conductivity for intervalley scattering [Eq. (16)], we fit the observed $\rho_{ab}(T)$ by the following formula

$$\rho_{ab} = \frac{c}{e^2}\left(\frac{1}{\tau_0} + \alpha T\right)\frac{1}{\varepsilon^*} + \frac{c}{e^2}\frac{1}{a_0 T\bar{\tau}}\exp\left(-\frac{\omega_0}{T}\right), \quad (17)$$

where $a_0 = 2\left(4\ln 2 - 1\right)/3\pi \approx 0.376$ and $\varepsilon^* \equiv c\int d^3k v_{\parallel}^2\left(-\partial f_{\mathbf{k}}^0/\partial\varepsilon_{\mathbf{k}}\right)/2\pi^3$. The first term in Eq. (17) accounts mostly for the low-T behavior of ρ_{ab}, when scattering at impurities ($1/\tau_0$) and soft phonons (αT) dominate transport. When calculating ε^*, we accounted for hopping between next-to-nearest planes, described by $\gamma_2 \approx 0.02$ eV. For finite γ_2, the Fermi energy is finite, $\epsilon^* \sim E_F$ at $T \to 0$, and the first term in Eq. (17) goes to a finite value at $T \to 0$. The second term is due to intervalley scattering. Equation (17) contains four fitting parameters: $\tau_0, \alpha, \bar{\tau}$, and ω_0. The results of the fit are shown in Fig. 1. The fitting parameters are $\tau_0 = 6.29 \times 10^{-12}$ s, $\alpha = 0.09$, $\bar{\tau} = 1.4\times 10^{-14}$ s, and $\omega_0 = 0.22$ eV. The values of τ_0 and α are in reasonable agreement with those found previously.[12] The frequency ω_0 is somewhat higher but still close to the frequency of the E_{2g} mode.[17,18] A rather short nominal time $\bar{\tau}$ indicates strong coupling between electrons and optical phonons in graphite.

For completeness, we note that for T above the Debye frequency, the multi-phonon processes modify the scattering rate as $1/\tau = 1/\tau_0 + \alpha\left(T + (T/T_2)^2 + (T/T_3)^3 + \mathcal{O}(T^4)\right)$, where $T_{2,3}$ correspond to an energy scale at which anharmonicity becomes strong. The data can be fitted by $T_2 \approx T_3 \approx 10^3$ K, which is well below the scale of 10^4 K at which anharmonicity becomes strong in other physical properties, such as the c-axis thermal expansion coefficient and elastic moduli.[20] This reinforces our conclusion that anharmonicity is not important in transport for $T < 1000$K.

IV. CONCLUSIONS

To summarize, we have studied, both experimentally and theoretically, the in-plane resistivity of HOPG. We found that its temperature dependence is determined by a competition between those of the carrier number density, $n(T)$, and of the scattering rate $1/\tau$. At temperatures below 50 K, the number density is practically independent of the temperature, while the the scattering rate increases with the temperature; as a result, the resistivity increases with T. At temperatures comparable to the Fermi energy, the increase in $n(T)$ almost compensates for that in $1/\tau$, leading to a quasi-saturation of ρ_{ab} at $T \sim 300$ K. However, full saturation never occurs because, as the temperature increases further, scattering off hard optical phonons, characterized by an exponential increase of $1/\tau$ with T, becomes important. This results in a further increase of ρ_{ab} with T.

[1] N. B. Brandt, S. M. Chudinov, and Ya. G. Ponomarev, *Semimetals: I. Graphite and its compounds,* (North-Holland, Amsterdam, 1988).

[2] H. Kempa, P. Esquinazi, and Y. Kopelevich, Solid State Communications **138**, 118 (2006).

[3] P. R. Wallace, Phys. Rev **71**, 622 (1947).

[4] At energies larger than γ_1, accessible in optical experiments, graphite can be viewed as a stack of decoupled graphene layers.

[5] E. G. Steward, B. P. Cook and E. A. Kellett, Nature **187**, 1015 (1960).

[6] N. Mounet and N. Marzari, Phys. Rev. B **71**, 205214 (2005).

[7] A similar consideration for the c-axis conductivity leads to a logarithmic divergence in σ_c: $\sigma_c \propto T^2\ln T$ (Ref. 3).

[8] E. McCann and V. I. Fal'ko, Phys. Rev. Lett. 96, 086805 (2006); J. Nilsson et al., Phys. Rev. B 73, 214418 (2006).

[9] C. A. Kukkonen and P. F. Maldague, Phys. Rev. Lett. **37**,

782 (1976).

[10] V. F. Gantmakher and Y. B. Levinson, *Scattering in metals and semiconductors* (North-Holland, 1987).

[11] D. T. Morelli and C. Uher, Phys. Rev. B **30**, 1080 (1984).

[12] X. Du, S.-W.Tsai, D. L. Maslov, and A. F. Hebard, Phys. Rev. Lett. **94**, 166601 (2005).

[13] S. Tongay, J. Hwang, D. B. Tanner, D. L. Maslov, and A. F. Hebard (unpublished).

[14] H. Veghaus, Phys. Stat. Sol. (b) **81**, 221 (1977).

[15] The equipartition theorem of the classical statistical physics, which states that the kinetic energy associated with every degree of freedom is equal to $T/2$, is not applicable to a compensated semimetal (even if the spectrum massive), because the distribution function is not Maxwellian but rather a Fermi-Dirac one with zero chemical potential.

[16] J. González, F. Guinea, and M. A. Vozmediano, Phys. Rev. B **59**, R2474 (1999).

[17] L. Wirtz and A. Rubio, Solid State Comm. **131**, 141 (2004).

[18] J. Maultzsch, S. Reich, C. Thomsen, H. Requardt, and P. Ordejòn, Phys. Rev. Lett. **92**, 075501 (2004).

[19] E. Mariani and F. von Oppen, Phys. Rev. Lett. **100**, 076801 (2008); ibid, **100**, 249901 (2008).

[20] T. Nihira and T. Iwata, Phys. Rev. B **68**, 134305 (2003).

[21] H. Suzuura and T. Ando, Phys. Rev. B **65**, 235412.

[22] A. H. Castro Neto and F. Guinea Phys. Rev. B **75**, 045404 (2007).